Hindawi
Advances in Meteorology
Volume 2019, Article ID 1257910, 11 pages
https://doi.org/10.1155/2019/1257910

Research Article

Effects of Environmental Factors on Ozone Flux over a Wheat Field Modeled with an Artificial Neural Network

Zhilin Zhu [1,2]

[1] *Key Laboratory of Ecosystem Network Observation and Modeling, Institute of Geographic Sciences and Natural Resources Research, Chinese Academy of Sciences, Beijing 100101, China*
[2] *College of Resources and Environment, University of Chinese Academy of Sciences, Beijing 100049, China*

Correspondence should be addressed to Zhilin Zhu; zhuzl@igsnrr.ac.cn

Received 24 January 2019; Revised 11 May 2019; Accepted 22 May 2019; Published 4 June 2019

Academic Editor: Ilan Levy

Ozone (O_3) flux-based indices are considered better than O_3 concentration-based indices in assessing the effects of ground O_3 on ecosystem and crop yields. However, O_3 flux (F_o) measurements are often lacking due to technical reasons and environmental conditions. This hampers the calculation of flux-based indices. In this paper, an artificial neural network (ANN) method was attempted to simulate the relationships between F_o and environmental factors measured over a wheat field in Yucheng, China. The results show that the ANN-modeled F_o values were in good agreement with the measured F_o values. The R^2 of an ANN model with 6 routine independent environmental variables exceeded 0.8 for training datasets, and the RMSE and MAE were 3.074 nmol·m^{-2}·s and 2.276 nmol·m^{-2}·s for test dataset, respectively. CO_2 flux and water vapor flux have strong correlations with F_o and could improve the fitness of ANN models. Besides the combinations of included variables and selection of training data, the number of neurons is also a source of uncertainties in an ANN model. The fitness of the modeled F_o was sensitive to the neuron number when it ranged from 1 to 10. The ANN model consists of complex arithmetic expressions between F_o and independent variables, and the response analysis shows that the model can reflect their basic physical relationships and importance. O_3 concentration, global radiation, and wind speed are the important factors affecting O_3 deposition. ANN methods exhibit significant value for filling the gaps of F_o measured with micrometeorological methods.

1. Introduction

In an atmospheric column, approximately 90% of total ozone (O_3) exists in the stratospheric O_3 layer and protects Earth's surface from excessive UV radiation. This category of O_3 is therefore referred to as "good" ozone [1]. However, the troposphere O_3 can negatively affect vegetation tissues, photosynthesis, and crop yields [2]. The tropospheric O_3 mainly results from the *in situ* photochemical production, and a small portion is transported from the stratosphere [3]. O_3 destruction involves chemical decomposition and deposition on Earth's surface. The total O_3 deposition can be quantitatively reflected by measured O_3 flux (F_o), and its magnitude and variations can facilitate understanding of the O_3 deposition processes.

The quantitative assessment of the effects of ground O_3 on ecosystem and crop yield loss in a region requires selection of an assessment model and calculation of the corresponding assessment index, and the calculation of assessment indices requires continuous measurement of O_3 concentration or flux [4, 5]. The concentration-based indices do not consider the status of vegetation and ecosystems (e.g., stomatal conductance and leaf area index). Many studies have shown that O_3-reduced yield loss is more closely related to the stomatal O_3 flux [5–7].

Gerosa et al. [8] presented a method of estimating O_3 stomatal flux by partitioning total F_o. Briefly, O_3 stomatal resistance was obtained by converting vapor stomatal resistance (Penman–Monteith approach), and the O_3 concentration near the canopy was calculated using the resistance

model, which needs the total O_3 flux. So, measuring total F_o is the first step in estimating stomatal O_3 flux [9]. F_o is usually measured by micrometeorological methods, and the eddy covariance (EC) method is considered the most direct flux-measuring method [8, 10–12]. However, due to a lack of high performance fast-response O_3 analyzers (e.g., it needs to change O_3-sensitive dye often and its sensitivity is unstable), EC-measured O_3 flux has many temporal gaps in the associated datasets [8, 13, 14]. This leads to difficulties in calculating the value of a O_3 stomatal flux-based index using the EC O_3 flux since the effect of O_3 on crop yields results from the accumulation of O_3 damage. Therefore, it is necessary to find a method of filling the gaps in O_3 flux datasets.

The gap-filling methods for ecosystem CO_2 flux have been summarized in the literature [15, 16]. However, there have not been investigations into methods for filling gaps in F_o data. As the controlling factors for O_3 flux are more complex, it is difficult to produce physically based equations to reflect the F_o and environmental variables under any conditions. Although some mechanism-based models (typically a resistance-in-series) have been developed, many parameters must be empirically estimated based on the specific site or type of vegetation [17, 18].

Artificial neural networks (ANN), as an artificial intelligence using machine learning techniques, have been applied for approximation, prediction, classification, modeling, and data gap-filling in many scientific disciplines [16, 19–21]. ANN is able to learn from training data and to represent the nonlinearity between the dependent and independent variables. It is suitable for simulating empirical datasets with complex and nonlinear relationships between variables and dependent variable(s). It is particularly useful when it is difficult to express these relationships using one or more simple equations. Compared to physically based models, ANNs have more success in simulating complex processes with a high precision without any analytical models [22–24]. These attributes make ANNs a good candidate for attempts at filling gaps in O_3 flux data. In addition, a sensitivity analysis can be conducted by analyzing the response curves of the different input variables that are created by fixing all other input variables at a certain value [25, 26]. For gap filling of F_o, ANN modeling is also a practical and simple method [16].

ANN methods have been used widely to model and predict O_3 concentration [27, 28] and CO_2 fluxes [21, 29, 30]. However, the ANN approach has not been used to simulate O_3 flux variation with other factor fluxes or meteorological factors. The objectives of this study are to (1) develop a series of ANN models to simulate the relationship between F_o and environmental variables; (2) determine the optimal ANN model to simulate F_o for interpolation of measured F_o; and (3) analyze the responses and relative importance of different environmental variables to O_3 flux.

2. Materials and Methods

2.1. Site and Observations. The observations were carried out over a winter wheat field at the Yucheng Comprehensive Experiment Station of the Chinese Academy of Sciences (36°50′N, 116°34′E; 28 m a.s.l.; Shandong Province, China). The site is located in the Northwest-Shandong plain, characterized by loamy soil texture and semiarid and warm temperate climate. The experimental site is very flat, and the fetch requirements for EC measurements are met. The study period of the field experiment covered entire growing season of wheat (from 2 March to 6 June 2012).

The ambient O_3 concentration was measured with a slow-response UV absorption-based O_3 analyzer (Model 205, 2B Technologies Inc., USA). The O_3 flux was measured with the eddy covariance method in combination with observations of CO_2, H_2O, and sensible heat fluxes. These variables were measured with a 3D sonic anemometer (CSAT3, Campbell Scientific Instrument, USA) and an open-path CO_2/H_2O gas analyzer (LI-7500, LI-COR Biosciences, USA). The O_3 fluctuation was measured with a fast-response O_3 analyzer developed by Enviscope GmbH [31] (hereafter referred to as ENVI). Micrometeorological and radiation variables measurements include air temperature and relative humidity (HMP45C; Vaisala Co., Finland), wind speed (A100R; Vector Instruments, UK), net radiation (CNR1; Kipp and Zonen, the Netherlands), and photosynthetically active radiation (LI-190SB; LI-COR, USA). All sensors were installed at 2.2 m height. Because of the continuous consumption of organic dye, the sensitivity of the ENVI slowly decreased with time. To maintain high sensitivity in the ENVI, we replaced the organic dye disc every 3 to 4 days. Raw data from the EC system were recorded at 10 Hz, and 30-minute mean data were recorded by a data logger (CR3000, Campbell Sci., USA).

2.2. O_3 Flux Calculation. Since the fast-response O_3 analyzer's sensitivity is not constant [14], the sensitivity must be calibrated by a slow-response O_3 concentration analyzer. However, it has been shown that the sensitivity can be treated as constant when using a 30 min averaging interval [32]. This means that the ENVI's output X (in mV) is proportional to the absolute ambient O_3 concentration over a 30 min period. Based on this assumption, the O_3 deposition velocity (V_d), defined as the O_3 flux divided by O_3 concentration, can be calculated by the following equation [33]:

$$V_d = -\frac{F_o}{\overline{\rho_o}} = -\frac{\overline{w'V_G'}}{\overline{V_G}}, \quad (1)$$

where ρ_o is the O_3 mass density (or concentration; $\mu g \cdot m^{-3}$), w is the vertical wind speed ($m \cdot s^{-1}$), and V_G is the output signal (mV) of the fast-response O_3 analyzer. The overbar denotes the time average, and the primes indicate the temporal fluctuation of each variable. The O_3 vertical turbulent flux F_o ($\mu g \cdot s^{-1} \cdot m^{-2}$) between atmosphere and surface is calculated by the following equation:

$$F_o = -\overline{\rho_o} V_d = \frac{P}{T}\frac{M_{o3}}{R}\frac{\overline{x_o}}{\overline{V_G}}\overline{w'V_G'}, \quad (2)$$

where x_o is the mean O_3 mixing ratio (ppb) measured by the slow-response O_3 analyzer, P is the barometric pressure ($N \cdot m^{-2}$), T is the air temperature (K), R is the universal gas constant ($8.314\ J \cdot mol^{-1} \cdot K^{-1}$), and M_{o3} is the molar mass of O_3 ($48.0\ g \cdot mol^{-1}$).

In practice, all fluxes were calculated by EddyPro® software with a series of corrections. Double rotation was utilized to correct tilt errors [34]. O_3 flux loss caused by time delay was corrected by the maximum covariance method [35]. Only the effect of density variation caused by water vapor on O_3 flux was considered [14, 36]. The more detailed description of observations, calculations, and corrections can be found in Zhu et al. [14].

2.3. Artificial Neural Network Modeling. In a general model, variable(s) and the independent variable can be expressed as one or more analytical expression(s). In contrast, artificial neural networks (ANNs) are capable of recognizing and simulating complex relations without any analytical expression(s) of variables and outputs. The relation is produced by the ANN that has been trained. Although there are many types of ANN (e.g., Hopfield networks and Kohonen networks) and many algorithms to be used to train ANN, the feedforward network (FFN) with backpropagation (BP) algorithm is the most popular and has been used in more than other types of neural networks for a wide variety of problems [26, 37–40]. The feedforward BP networks have a simple structure for simulating complex systems, and its structure is sufficiently robust to simulate many nonlinear systems [27, 41]. Therefore, the BP network was used in the study. Figure 1 shows a schematic of the three-layer BP network. The nonlinear elements or neurons are arranged in successive layers, and the information flows from input layer to output layer through the hidden layers. The number of inputs depends on the model performance, and theoretically, more inputs increase model performance. The hidden layers are another important parameter in a BP network.

Because of the complexity of the ANN calculation process, the ANN core algorithms used in this study are adopted from the MATLAB software package. However, the ANN requires a prepared dataset and the determination of parameters. The general steps for the setup of the BP network and parameters are described as follows:

(1) *The determination of independent variables* (X_i, $i = 1, 2, \ldots, n$). Although ANNs do not require the specification of dependent variables and independent variables, variables should have a certain relationship in terms of mechanism(s) or variation patterns. Based on the previous studies and observed items, we attempt to build a series of ANN models. These models have different combinations of input variables to determine the most relevant input variables for modeling O_3 flux. The input variables include micrometeorological variables, radiation values, and fluxes.

(2) *The determination of the number of nodes or "neurons" in the hidden layer.* This is related to experience or examinations. In general, this number should be larger than the number of X_i.

(3) *The generation of a network by training.* The training dataset and parameters are the keys to generate a good BP network. The training dataset must be representative and of high quality, and the parameters should be suitable. The training process will determine a set of optimal weights and biases. Although there are different transfer functions, such as linear function and a threshold function [38], sigmoid transfer function is the most popular choice for many studies [40]. This transfer function was also used for the neurons in the hidden layer. Using the MATLAB software package, the weights and biases in the ANN are obtained in an iterative calibration process based on the Levenberg-Marquardt (LM) algorithm. The root-mean-squared error is used to monitor the performance of modeling. Normally, the validation error decreases during the initial phase of training and begins to rise when the network begins to overfit the data. To avoid overfitting, the weights and biases of the network can be automatically saved when the validation error reaches a minimum.

(4) *The evaluation of the ANN model using training and test datasets.* In this study, three statistical parameters, i.e., root-mean-squared error (RMSE), mean absolute error (MAE), and coefficient of determination (R^2), were used to evaluate the performance of models. RMSE and MAE present information about the degree of accuracy of an ANN model, and R^2 measures the degree of the linear relationship between measured and modeled O_3 fluxes.

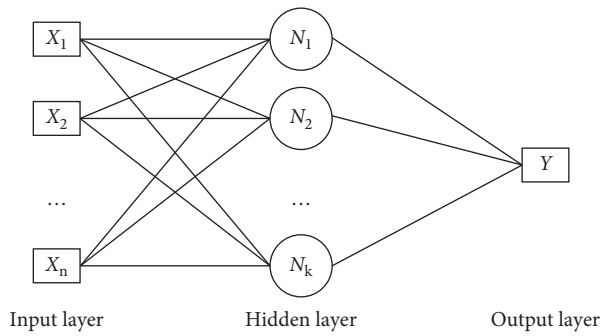

Figure 1: Schematic of a three-layer backpropagation artificial neural network.

The three parameters were calculated with the following equations:

$$\mathrm{RMSE} = \sqrt{\frac{1}{N}\sum_{i=1}^{N}\left(Y_i - F_i\right)^2},$$

$$\mathrm{MAE} = \frac{1}{N}\sum_{i=1}^{N}\left|Y_i - F\right|, \tag{3}$$

$$R^2 = \frac{\left[\sum\left(Y_i - \overline{Y}\right)\left(F_i - \overline{F}\right)\right]^2}{\sum\left(Y_i - \overline{Y}\right)\sum\left(F_i - \overline{F}\right)},$$

where Y_i and F_i are the simulated and measured O_3 flux, respectively; the overbar denotes the average of each variables, and N is the sample number.

2.4. Dataset Preparation. To create a satisfactory ANN model, a high-quality dataset is very important. Due to different reasons, all variables, especially the measured O_3 flux, presented many low quality or erroneous data. In this study, the selected data for training and testing satisfy the conditions as follows. Approximately 58.5% of the total data points in the set are low quality or erroneous, and they were filtered using the following metrics.

(1) Only daytime data were adopted. During nighttime, O_3 concentration is generally low and wheat stomata are closed, and the effect of O_3 on wheat can be ignored. Nighttime fluxes also exhibit a significant amount of inaccuracies because of weak turbulence [42].

(2) Ozone fluxes are between $-40\,\mathrm{nmol{\cdot}m^{-2}{\cdot}s^{-1}}$ and $0\,\mathrm{nmol\,m^{-2}{\cdot}s^{-1}}$. As O_3 is always deposited downward on the surface, the positive O_3 fluxes represent errors. The initial threshold value of $-40\,\mathrm{nmol{\cdot}m^{-2}{\cdot}s^{-1}}$ was empirically determined via the time series of O_3 flux. Moreover, the threshold was variable based on the wheat status. For example, the threshold was set to $-20\,\mathrm{nmol{\cdot}m^{-2}{\cdot}s^{-1}}$ in the first stage of wheat. In addition, some rapid spikes of O_3 flux were deemed unlikely based on the underlying mechanisms. These data points were deleted even though they did not exceed the threshold value.

(3) The data of all inputs at a time are completed. Some input variables, especially the turbulent fluxes, have errors or gaps due to various reasons. To keep training data consistent, these data were also excluded.

Finally, 1402 data points (41.5% of total O_3 flux data) were used to train and validate all ANN models. Half of the high-quality dataset (701 data points) was selected for ANN training, and the other half of-high quality data were used for the test dataset. According to the MATLAB software manual, the training dataset is randomly divided into three subsets, i.e., the training set, the validation set, and the test set. Their ratios are 70%, 15%, and 15%, and the corresponding data points are 491, 105, and 105, respectively. The training set is used for computing the gradient as well as updating the network weights and biases. The validation set is used to validate the ANN performance, and the test set is used to compare different models.

3. Results and Discussion

3.1. Input Variables Choice and Its Performances. Although an ANN model is only dependent on the mathematical relations of inputs and outputs, variables that are irrelevant or lack a physical basis should be excluded. Based on equation (1), O_3 flux is the product of O_3 concentration and deposition velocity (V_d). For O_3 concentration, the production and decomposition result from a series of complex chemical and physical processes. The local O_3 concentration variation mainly depends on its precursors (e.g., VOCs and NO_x), long-range transport and a subset of environmental factors, such as radiation, temperature, and humidity [43–45]. V_d is affected to a certain extent by atmospheric turbulence intensity and underlying surface conditions, such as wind speed, friction speed, soil moisture, O_3-reactive chemicals, and vegetation status [46–48].

Due to a lack of observations for O_3-reactive chemicals, only some micrometeorological and radiation variables were selected to model F_o variation in this study. The initial input variables for attempting to model F_o include O_3 concentration (C_{O_3}), global radiation (Q), air temperature (T_a), relative humidity (RH), wind speed (U), and soil water content (S_W). In addition, O_3 flux access to stomata is coupled with the CO_2 flux (F_c) and water vapor fluxes (LE). These two fluxes are also deployed in our attempts to model F_o. Because of the high correlation between the mean diurnal pattern of many variables and time [30], the effect of time (T_m) on the ANN model was also investigated in this study.

To test the dependency of each variable on O_3 flux, the O_3 flux with one variable was first simulated, and then, O_3 flux with different variable combinations were simulated. Table 1 presents the statistics for each variable and variable combinations. For any single micrometeorological variable, the RMSE values exceed $5\,\mathrm{ng{\cdot}m^{-2}{\cdot}s^{-1}}$ and all R^2 values are less than 0.4. This means that any single variable cannot accurately model O_3 flux. Among these variables, O_3 concentration and radiation have relatively strong correlations. For other turbulent fluxes (LE, F_c), ANN-modeled F_o values were strongly correlated with F_c and LE, but modeled F_o values were weakly correlated with sensible heat flux (H). This highlights the fact that O_3 flux is mainly affected by the stomata flux, as stomata are the main pathway of LE and F_c. Although these fluxes have similar diurnal patterns, F_c and LE cannot be considered as the driving factors of O_3 deposition. The O_3 deposition process is complex, and changes in the process are mainly driven by many meteorological or environmental factors.

To obtain an optimal ANN model, we attempted to build more ANN models with different combinations of input variables. The combinations can be divided into two classes. Class 1 combinations only consist of routine micrometeorological and radiation factors (T_a, RH, U, Q, S_W, and C_{O_3}), i.e., models T11 to T15 in Table 1. Meanwhile, we also tested the effect of time (T16). The variables in Class 1 are easy to observe and possess sufficiently high accuracy. The combinations can increase the fitness of observed and ANN-modeled F_o, even if the combination only uses meteorological variables (T12). Class 2 combinations add the turbulent fluxes (H, F_c, and LE) in addition to the variables in Class 1, i.e., models T17 to T20 in Table 1. Although the correlation levels increase slightly in Class 2 models when compared to the models of Class 1, the effect of these fluxes on F_o gap filling is very limited. When there is a gap in F_o data, other fluxes (F_c and LE) often exhibit simultaneous gaps in their observational datasets. Meanwhile, the flux data have lower accuracies than the micrometeorological and

Table 1: Statistics for each ANN model with training dataset and test dataset.

Model	Inputs and combinations	Training dataset			Test dataset		
		RSME (nmol·m^{-2}·s)	MAE (nmol·m^{-2}·s)	R^2	RSME (nmol·m^{-2}·s)	MAE (nmol·m^{-2}·s)	R^2
T1	T_a	5.391	4.119	0.282	5.578	4.305	0.234
T2	RH	6.251	4.780	0.062	6.252	4.808	0.059
T3	U	5.897	4.495	0.141	5.974	4.558	0.123
T4	Q	5.339	4.044	0.301	5.607	4.226	0.237
T5	S_W	6.091	4.589	0.109	6.183	4.683	0.090
T6	C_{O_3}	5.182	3.836	0.338	5.394	4.015	0.287
T7	H	6.229	4.786	0.040	6.537	4.887	0.009
T8	LE	4.273	3.289	0.551	4.731	3.591	0.461
T9	F_c	5.075	3.678	0.381	5.496	4.035	0.294
T10	T_m	5.817	4.326	0.171	5.831	4.295	0.163
T11	T_a RH	5.205	3.864	0.330	5.365	4.045	0.289
T12	T_a RH U	4.013	3.033	0.604	4.177	3.172	0.571
T13	T_a RH U Q	3.723	2.792	0.659	3.929	2.926	0.621
T14	T_a RH U Q S_W	3.569	2.667	0.685	3.752	2.798	0.652
T15	T_a RH U Q S_W C_{O_3}	2.662	1.971	0.827	3.074	2.276	0.767
T16	T_a RH U Q S_W C_{O_3} T_m	2.652	1.967	0.829	3.021	2.215	0.783
T17	T_a RH U Q S_W C_{O_3} H	2.460	1.813	0.855	2.844	2.055	0.805
T18	T_a RH U Q S_W C_{O_3} LE	2.448	1.812	0.855	2.834	2.079	0.809
T19	T_a RH U Q S_W C_{O_3} F_c	2.254	1.671	0.875	2.763	1.997	0.814
T20	T_a RH U Q S_W C_{O_3} LE F_c	2.310	1.662	0.881	2.697	1.917	0.839

radiation variables. Among the two classes of combinations, we select T15 and T20 as examples to analyze their performances as well as the contributions and responses of each variable to O_3 flux.

Figure 2 shows a scatter plot of measured and modeled O_3 fluxes using ANN models T15 and T20 for the training dataset and test dataset. The modeled O_3 fluxes in these two models match the measured O_3 flux to a high degree. There are not obvious deviations from the 1 : 1 line. Although the first model contains only six routine variables (no turbulent fluxes), the model produced an R^2 of 0.826 and 0.767 for the training dataset and test dataset, respectively. The fitness of model T20 is marginally superior to the fitness of T15. The R^2 values of T20 are 0.881 and 0.839 for the training dataset and test dataset, respectively. The R^2 can be interpreted as the ratio of the variances for the modeled flux and the real flux.

3.2. Effect of ANN Schema on the Model Performance. In addition to the selection of variable combinations, the training data quality and architecture parameters also affect the performance of an ANN model. The ANN model can be considered as a black-box, so the performance is strongly dependent on the training dataset quality. Network architecture consists of numbers of layers, number of nodes, and weight calculation method. Generally, greater numbers of layers and nodes produce better performance. However, to avoid overtraining, the ANN training process requires an appropriate learning rate (weight adjustment steps) and a stopping criterion [16].

Compared to other types of statistical models, ANN models are difficult to replicate. Even if the same dataset and parameters are used, there are slight differences in the modeled results between different runs. The results after training vary slightly because the neural network is initialized with random weights. As an example, Figure 3 shows the daily variations of O_3 flux measured on May 12 with EC method and ANN modeled with T15. It is clear that the ANN modeled F_o each run are different, and they are around the measured F_o. To mitigate these uncertainties, we calculated the average of 10 runs with the same variables combinations and parameters to generate the modeled O_3 flux. Table 2 compares the statistics of ANN-modeled F_o with T15. As shown, statistical indicators of 10-run-averaged are better than separate indicators. The RMSE and MAE are the smallest, and the R^2 is the largest.

Another problem that arises in ANN modeling is so-called overtraining or overfitting. An overtrained network cannot learn the general traits that exist in the training set, and the network will lose the capacity to generalize. Three important parameters can be used to avoid this phenomenon: the number of hidden layers, the number of epochs, and the number of neurons in each hidden layer. Although these parameters are crucial to a model, there are no definite rules on how to determine them. In the ANN package of the MATLAB software, the number of hidden layers and the number of neurons in each hidden layer can be assigned. To decrease the number of ANN parameters, a feedforward network with one hidden layer and a sufficient number of neurons was used in this study. This satisfies any finite input-output statistical modeling [41]. The optimal number of epochs (iterations) can be determined automatically by the software based on the best performances. Therefore, only the optimum neurons should be determined by testing the performance of an ANN model with different neurons.

Figure 4 shows the variations of MAE, RMSE, and R^2 for the models T15 and T20 as the number of neurons change. It can be seen that the MAE and RMSE of the two ANN models rapidly decrease when the number of neurons changes from 1 to 10, and then the variations are slower and more stable.

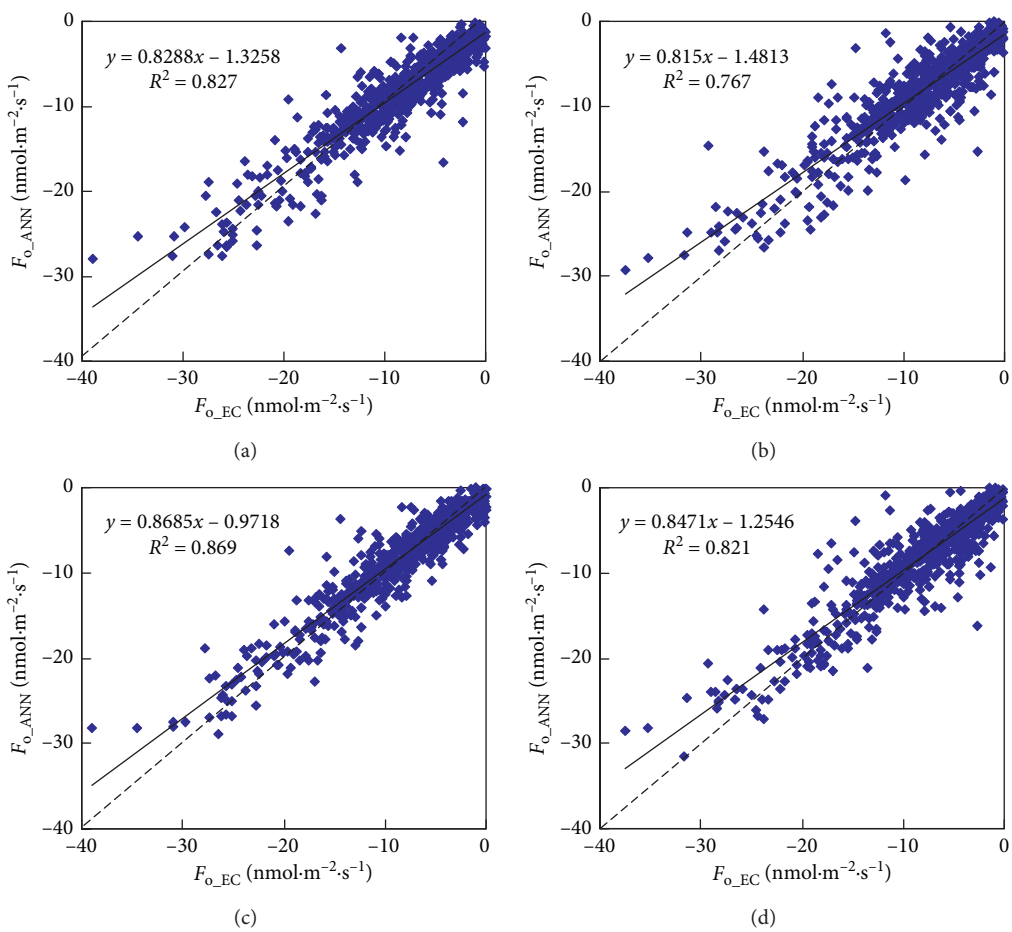

Figure 2: Observed versus simulated ozone flux with models T15 and T20, respectively. (a) Model T15 with the training dataset. (b) Model T15 with the test dataset. (c) Model T20 with the training dataset. (d) Model T20 with the test dataset.

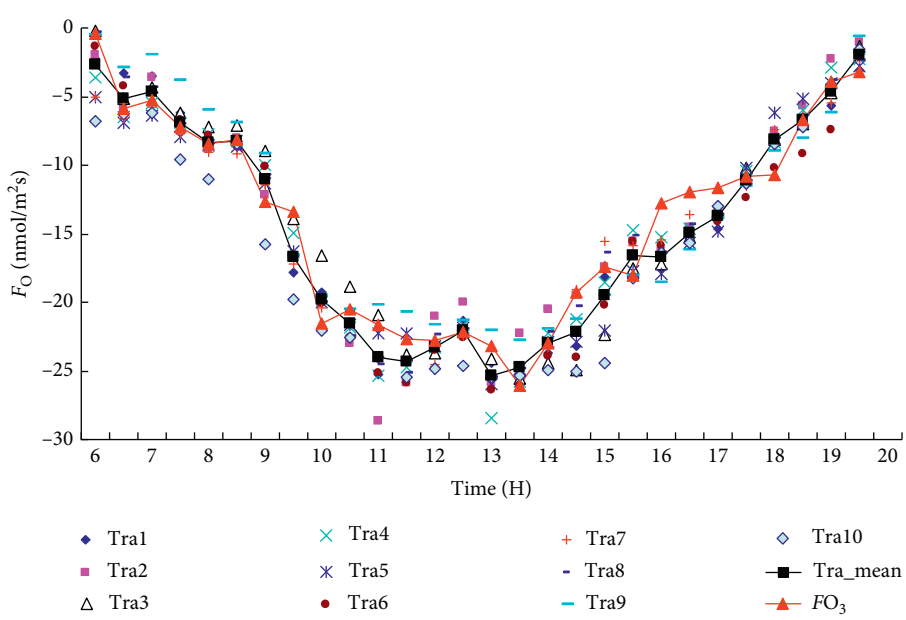

Figure 3: Comparison of diurnal variations of ozone flux measured on May 12 with the EC method (F_{O_3}) and 10-run ANN modeled with T15. Tra_mean is the mean of 10 runs in the ANN model of F_o.

Table 2: Comparison of statistics of F_o values from measurements and the ANN model (T15) in 10 separate runs.

	Tra1	Tra2	Tra3	Tra4	Tra5	Tra6	Tra7	Tra8	Tra9	Tra10	T_mean
RMSE (nmol·m^{-2}·s)	2.861	2.715	2.829	2.738	2.837	2.798	2.789	2.77	2.754	2.789	2.662
MAE (nmol·m^{-2}·s)	2.191	2.078	2.148	2.155	2.174	2.115	2.044	2.135	2.071	2.091	1.971
R^2	0.808	0.802	0.802	0.809	0.795	0.798	0.811	0.813	0.819	0.812	0.827

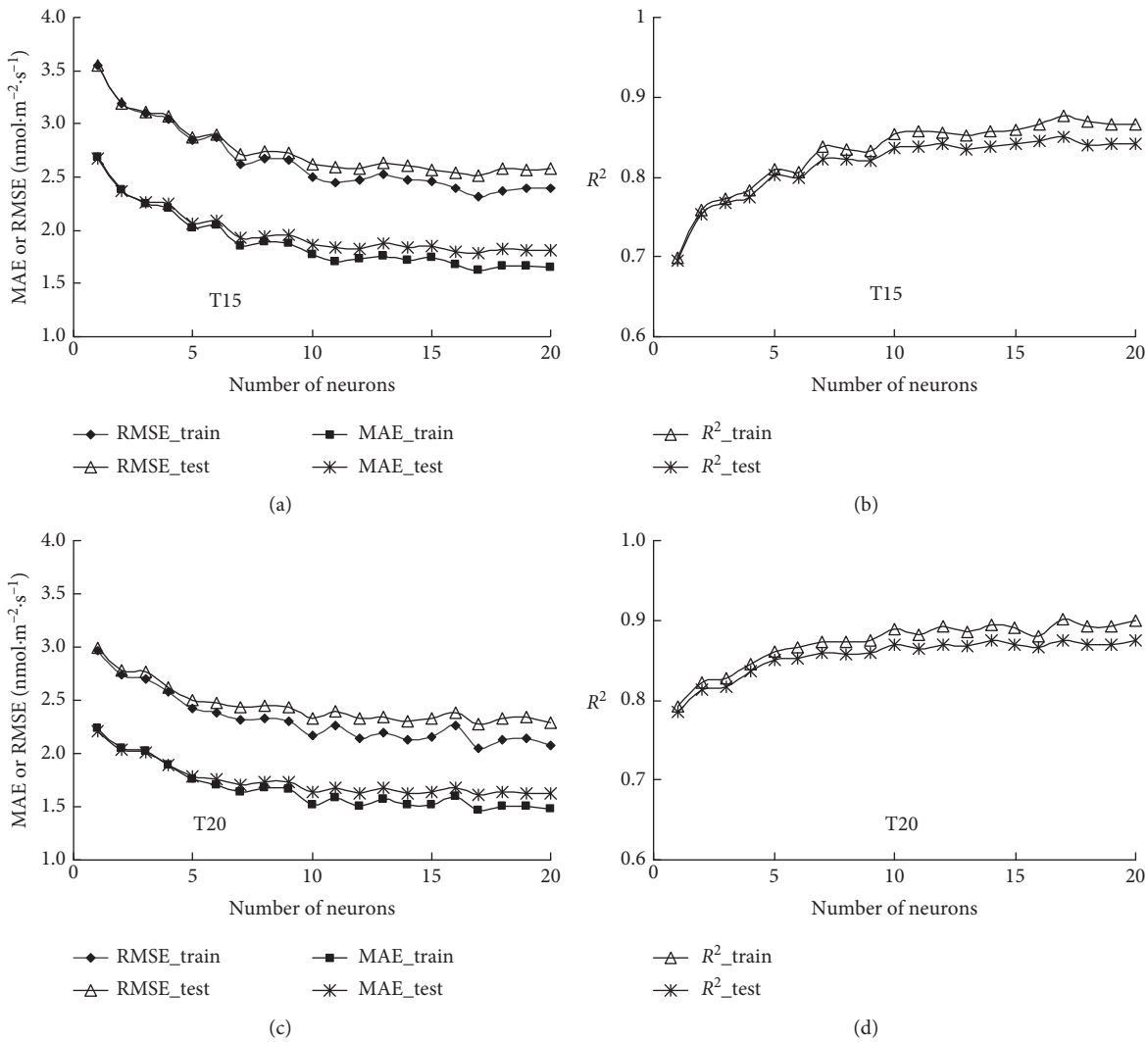

Figure 4: Variations of MAE, RMSE, and R^2 for the models T15 and T20 with different numbers of neurons.

The minima for MAE and RMSE appeared when there were 17 neurons. The performance of R^2 is similar (Figures 4(b) and 4(d)). Therefore, the number 17 was determined to be the optimal neuron number for the hidden layer in our analysis.

3.3. Response of F_o to Variables Based on ANN Models. All parameters of an ANN model are fixed once training is finished. The responses of an ANN model can be evaluated by varying a single variable within its measured range and keeping other inputs fixed at their mean values [30, 37]. Figure 5 demonstrates the details of how O_3 flux varies across the range of all variables within models T15 and T20. The ranges (minimum and maximum) and mean values of each input variables in the training dataset are given in Table 3.

By excluding the effects of turbulent fluxes, the effect of each environmental variable on F_o can be seen more clearly (Figure 5(a)). Positive responses between O_3 concentration, temperature, solar radiation, and relative humidity are shown clearly. After considering the effects of turbulent fluxes (Figure 5(b)), the responses of F_c and LE are very obvious, whereas the responses of T_a, RH, and S_W are very weak. Moreover, O_3 flux shows a unidirectional variation with most variables, such as O_3 concentration, wind speed, temperature, and humidity. Nevertheless, the variation of F_o with soil water content (S_W) shows a different pattern (Figure 5(a)). O_3 deposition decreased when soil water

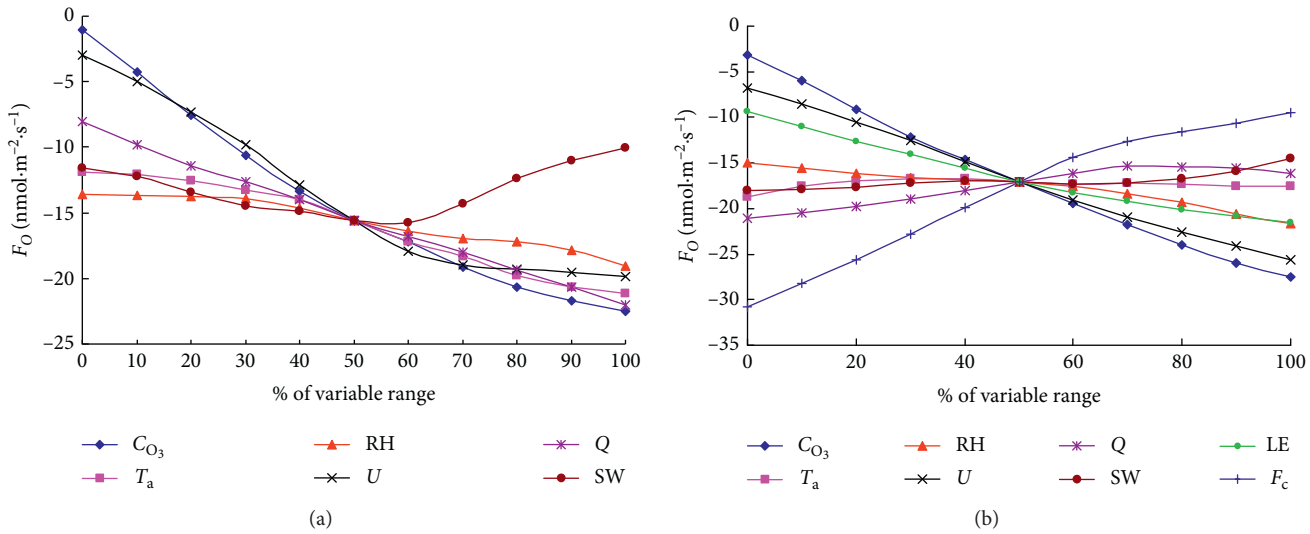

Figure 5: Responses and relative importance of each variable in the ANN models T15 and T20.

Table 3: Input parameters and their ranges for different models.

Variable	Unit	Min	Max	Mean
Air temperature (T_a)	C	−5.4	30.6	12.6
Relative humidity (RH)	%	14	100	57
Wind speed (U)	m·s^{-1}	0	7.2	3.6
Ozone concentration (C_{O_3})	Ppb	1.0	124.2	62.6
Global radiation (Q)	W·m^{-2}	0	924	462
Sensible heat flux (H)	W·m^{-2}	−100	300	100
Latent heat flux (LE)	W·m^{-2}	0	560	280
CO_2 flux (F_c)	mg·m^2·s^{-1}	−2.2	0.2	−1.0

content was too high or too low. The results might be unreliable and should be explained carefully. One possible reason for this pattern is that the change in soil water content is slow over the course of a day and there is no clear diurnal variation. The response of S_W and F_o in the ANN models mainly reflects the long-term variation of O_3 flux. For other variables, the diurnal variation amplitude is larger than that of long-term variations. A simple expression that relates F_o and the various variables could not be given by the ANNs, as the response of F_o to a single variable may depend on the values of the other inputs. However, the response curves of variables can basically reflect the effect of each variable on O_3 flux.

The response curve can also reveal the importance of each variable [41]. This method is called the "profile method" [25]. In this study, the importance of each variable is described by comparing the variation ranges of modeled values when a variable is varied from its minimum to maximum and other variables are fixed at their mean values given in Table 3. A larger variation in F_o indicates a higher parameter importance. Excluding the effects of fluxes, the order of variable importance in model T15 is as follows: $C_{O_3} > U > Q > T_a > \mathrm{RH} > S_W$ (Figure 5(a)). O_3 concentration, wind speed, and radiation are the important factors affecting ozone deposition over wheat fields. In addition, to quantitatively reflect the effect of each variable, the relative importance (RI) of each variable was calculated [39, 49, 50]. The RI of C_{O_3}, U, Q, T_a, RH, and S_W are 26.7, 21.6, 20.6, 12.4, 11.3 and 7.4, respectively.

Using equation (2), it is easy to understand that the ozone concentration is the most important factor affecting ozone flux. Other factors controlling ozone deposition, such as solar radiation, temperature, humidity, and soil water content, have also been studied [47, 51]. Wind speed is another important factor affecting ozone deposition in this study. Although wind speed does not directly result in the increase of ozone deposition, it does enhance atmospheric turbulence. This causes more ozone in the air to enter crop stomata. In fact, radiation indirectly influences ozone deposition by influencing other model inputs. It results in the production of local ozone and leads to the changes in temperature, humidity, wind speed, and other environmental factors.

When considering the effects of fluxes, the order of variable importance in model T20 is as follows: $F_c > C_{O_3} > U > \mathrm{LE} > Q > T_a$ (Figure 5(b)). As most CO_2 and water vapor are exchanged via the same pathway of stomata [52, 53], there are strong corrections between F_o and other gas fluxes (F_c and LE). Stomatal uptake might play an important role in ozone deposition. In model T20, the effect of Q on ozone flux becomes small. This might be because the effects of radiation are replaced by these fluxes. In other words, when the effects of CO_2/H_2O fluxes are taken into account, the correlations between F_o and these fluxes are more significant than those between F_o and radiation.

4. Conclusions

Based on the EC-measured F_o and other environmental factors over a wheat field, an artificial neural network method was attempted to simulate the relationships between F_o and environmental factors. Our conclusions can be summarized as follows:

(1) Generally, more input variables can increase the performance of a model. By only using the routine

micrometeorological variables of radiation and O_3 concentration, we can create an ANN model to simulate the variation of F_o. The R^2 of a model with 6 routine independent variables can exceed 0.8 for the training dataset and test dataset. CO_2 flux and water vapor flux have strong corrections to F_o, and they can improve the fitness of the ANN models when they are considered as independent variables.

(2) In addition to variable combinations and training data, the model parameters (e.g., the number of neurons) are also a source of uncertainties in an ANN model. The effect of neuron number on our model fitness (MAE, RMSE, and R^2) is obvious when it changes from 1 to 10. Empirically, one hidden layer with 17 neurons produced the best results.

(3) The ANN model is composed of complex arithmetic expressions between F_o and independent variables, an optimal ANN model can roughly reflect their inner relationships and relative importance. Global radiation, O_3 concentration, and wind speed are the important factors that affect O_3 deposition. There are strong correlations between F_o and gas fluxes (F_c and LE). The ANN method represents a valuable route for filling the gaps of a time series of F_o during the experimental period with micrometeorological methods.

Data Availability

The MS-Excel data used to support the findings of this study are available from the corresponding author upon request.

Conflicts of Interest

The authors declare that they have no conflicts of interest.

Acknowledgments

This work was supported by the National Natural Science Foundation of China (grant number 41675147) and the National Key R&D program of China (grant number 2017YFC0503801). The author would also like to thank Accdon for providing linguistic assistance during the preparation and revision of this manuscript.

References

[1] R. A. Kerr, "Ozone depletion: a brighter outlook for good ozone," *Science*, vol. 297, no. 5587, pp. 1623–1625, 2002.

[2] X. Wang, Q. Zhang, F. Zheng et al., "Effects of elevated O3 concentration on winter wheat and rice yields in the Yangtze River Delta, China," *Environmental Pollution*, vol. 171, pp. 118–125, 2012.

[3] P. J. Crutzen, M. G. Lawrence, and U. Poschl, "On the background photochemistry of tropospheric ozone," *Tellus A*, vol. 51, no. 1, pp. 123–146, 1999.

[4] W. J. Massman, "Toward an ozone standard to protect vegetation based on effective dose: a review of deposition resistances and a possible metric," *Atmospheric Environment*, vol. 38, no. 15, pp. 2323–2337, 2004.

[5] E. Paoletti and W. J. Manning, "Toward a biologically significant and usable standard for ozone that will also protect plants," *Environmental Pollution*, vol. 150, no. 1, pp. 85–95, 2007.

[6] R. Musselman, A. Lefohn, W. Massman, and R. Heath, "A critical review and analysis of the use of exposure- and flux-based ozone indices for predicting vegetation effects," *Atmospheric Environment*, vol. 40, no. 10, pp. 1869–1888, 2006.

[7] H. Pleijel, H. Danielsson, K. Ojanperä et al., "Relationships between ozone exposure and yield loss in European wheat and potato-a comparison of concentration- and flux-based exposure indices," *Atmospheric Environment*, vol. 38, no. 15, pp. 2259–2269, 2004.

[8] G. Gerosa, S. Cieslik, and A. Ballarin-Denti, "Micrometeorological determination of time-integrated stomatal ozone fluxes over wheat: a case study in Northern Italy," *Atmospheric Environment*, vol. 37, no. 6, pp. 777–788, 2003.

[9] D. Fowler, C. Flechard, J. N. Cape, R. L. Storeton-West, and M. Coyle, "Measurements of ozone deposition to vegetation quantifying the flux, the stomatal and non-stomatal components," *Water, Air, and Soil Pollution*, vol. 130, no. 1–4, pp. 63–74, 2001.

[10] D. D. Baldocchi, "Measuring fluxes of trace gases and energy between ecosystems and the atmosphere-the state and future of the eddy covariance method," *Global Change Biology*, vol. 20, no. 12, pp. 3600–3609, 2014.

[11] E. Lamaud, A. Carrara, Y. Brunet, A. Lopez, and A. Druilhet, "Ozone fluxes above and within a pine forest canopy in dry and wet conditions," *Atmospheric Environment*, vol. 36, no. 1, pp. 77–88, 2002.

[12] E. Lamaud, B. Loubet, M. Irvine, P. Stella, E. Personne, and P. Cellier, "Partitioning of ozone deposition over a developed maize crop between stomatal and non-stomatal uptakes, using eddy-covariance flux measurements and modelling," *Agricultural and Forest Meteorology*, vol. 149, no. 9, pp. 1385–1396, 2009.

[13] T. N. Mikkelsen, H. Ro-Poulsen, M. F. Hovmand, N. O. Jensen, K. Pilegaard, and A. H. Egeløv, "Five-year measurements of ozone fluxes to a Danish Norway spruce canopy," *Atmospheric Environment*, vol. 38, no. 15, pp. 2361–2371, 2004.

[14] Z. Zhu, F. Zhao, L. Voss et al., "The effects of different calibration and frequency response correction methods on eddy covariance ozone flux measured with a dry chemiluminescence analyzer," *Agricultural and Forest Meteorology*, vol. 213, pp. 114–125, 2015.

[15] E. Falge, D. Baldocchi, R. Olson et al., "Gap filling strategies for defensible annual sums of net ecosystem exchange," *Agricultural and Forest Meteorology*, vol. 107, no. 1, pp. 43–69, 2001.

[16] A. M. Moffat, D. Papale, M. Reichstein et al., "Comprehensive comparison of gap-filling techniques for eddy covariance net carbon fluxes," *Agricultural and Forest Meteorology*, vol. 147, no. 3-4, pp. 209–232, 2007.

[17] M. L. Wesely, "Parameterization of surface resistances to gaseous dry deposition in regional-scale numerical models," *Atmospheric Environment*, vol. 23, no. 6, pp. 1293–1304, 1989.

[18] L. Zhang, J. R. Brook, and R. Vet, "On ozone dry deposition-with emphasis on non-stomatal uptake and wet canopies," *Atmospheric Environment*, vol. 36, no. 30, pp. 4787–4799, 2002.

[19] M. Aubinet, A. Grelle, A. Ibrom et al., "Estimates of the annual net carbon and water exchange of forests: the EUROFLUX

methodology," *Andvances in Ecological Research*, vol. 30, pp. 113–175, 2000.

[20] M. W. Gardner and S. R. Dorling, "Artificial neural networks (the multilayer perceptron)-a review of applications in the atmospheric sciences," *Atmospheric Environment*, vol. 32, no. 14-15, pp. 2627–2636, 1998.

[21] D. Papale and R. Valentini, "A new assessment of European forests carbon exchanges by eddy fluxes and artificial neural network spatialization," *Global Change Biology*, vol. 9, no. 4, pp. 525–535, 2003.

[22] G. R. Balls, D. Palmer-brown, and G. E. Sanders, "Investigating microclimatic influences on ozone injury in clover (*Trifolium subterraneum*) using artificial neural networks," *New Phytologist*, vol. 132, no. 2, pp. 271–280, 1996.

[23] A. C. Comrie, "Comparing neural networks and regression models for ozone forecasting," *Journal of the Air and Waste Management Association*, vol. 47, no. 6, pp. 653–663, 1997.

[24] J. M. Nicely, R. J. Salawitch, T. Canty et al., "Quantifying the causes of differences in tropospheric OH within global models," *Journal of Geophysical Research: Atmospheres*, vol. 122, no. 3, pp. 1983–2007, 2017.

[25] M. Gevrey, I. Dimopoulos, and S. Lek, "Review and comparison of methods to study the contribution of variables in artificial neural network models," *Ecological Modelling*, vol. 160, no. 3, pp. 249–264, 2003.

[26] J. A. Vrugt, W. Bouten, S. C. Dekker, and P. A. D. Musters, "Transpiration dynamics of an Austrian pine stand and its forest floor: identifying controlling conditions using artificial neural networks," *Advances in Water Resources*, vol. 25, no. 3, pp. 293–303, 2002.

[27] Y. Feng, W. Zhang, D. Sun, and L. Zhang, "Ozone concentration forecast method based on genetic algorithm optimized back propagation neural networks and support vector machine data classification," *Atmospheric Environment*, vol. 45, no. 11, pp. 1979–1985, 2011.

[28] J. C. M. Pires, B. Gonçalves, F. G. Azevedo et al., "Optimization of artificial neural network models through genetic algorithms for surface ozone concentration forecasting," *Environmental Science and Pollution Research*, vol. 19, no. 8, pp. 3228–3234, 2012.

[29] H. He, G. Yu, L. Zhang, X. Sun, and W. Su, "Simulating CO2 flux of three different ecosystems in ChinaFLUX based on artificial neural networks," *Science in China Series D: Earth Sciences*, vol. 49, no. S2, pp. 252–261, 2006.

[30] M. T. V. Wijk and W. Bouten, "Water and carbon fluxes above european coniferous forests modelled with artificial neural networks," *Ecological Modelling*, vol. 120, pp. 181–197, 1999.

[31] A. Zahn, J. Weppner, H. Widmann et al., "A fast and precise chemiluminescence ozone detector for eddy flux and airborne application," *Atmospheric Measurement Techniques*, vol. 5, no. 2, pp. 363–375, 2012.

[32] M. Ermel, R. Oswald, J.-C. Mayer et al., "Preparation methods to optimize the performance of sensor discs for fast chemiluminescence ozone analyzers," *Environmental Science and Technology*, vol. 47, no. 4, pp. 1930–1936, 2013.

[33] J. B. A. Muller, C. J. Percival, M. W. Gallagher, D. Fowler, M. Coyle, and E. Nemitz, "Sources of uncertainty in eddy covariance ozone flux measurements made by dry chemiluminescence fast response analysers," *Atmospheric Measurement Techniques*, vol. 3, no. 1, pp. 163–176, 2010.

[34] J. M. Wilczak, S. P. Oncley, and S. A. Stage, "Sonic anemometer tilt correction algorithms," *Boundary-Layer Meteorology*, vol. 99, no. 1, pp. 127–150, 2001.

[35] J. B. Moncrieff, J. M. Massheder, H. De Bruin et al., "A system to measure surface fluxes of momentum, sensible heat, water vapour and carbon dioxide," *Journal of Hydrology*, vol. 188-189, pp. 589–611, 1997.

[36] E. Webb, G. Pearman, and R. Leuning, "Correction of flux measurements for density effects due to heat and water vapour transfer," *Quarterly Journal of the Royal Meteorological Society*, vol. 106, no. 447, pp. 85–100, 1980.

[37] C. Huntingford and P. M. Cox, "Use of statistical and neural network techniques to detect how stomatal conductance responds to changes in the local environment," *Ecological Modelling*, vol. 97, no. 3, pp. 217–246, 1997.

[38] S. Lek, J. L. Giraudel, and J. P. Guegan, "Neuronal networks. Algorithms and architectures for ecologists and evolutionary ecologists," in *Artificial Neuronal Network: Application to Ecology and Evolution*, S. Lek and J. P. Guegan, Eds., Springer-Verlag Berlin, Heidelberg, New York, NY, USA, 2000.

[39] X. Dai, Z. Huo, and H. Wang, "Simulation for response of crop yield to soil moisture and salinity with artificial neural network," *Field Crops Research*, vol. 121, no. 3, pp. 441–449, 2011.

[40] G. Zhang, B. Eddy Patuwo, and Y. Hu M., "Forecasting with artificial neural networks:," *International Journal of Forecasting*, vol. 14, no. 1, pp. 35–62, 1998.

[41] S. Lek, M. Delacoste, P. Baran, I. Dimopoulos, J. Lauga, and S. Aulagnier, "Application of neural networks to modelling nonlinear relationships in ecology," *Ecological Modelling*, vol. 90, no. 1, pp. 39–52, 1996.

[42] G. Gerosa, R. Marzuoli, S. Cieslik, and A. Ballarin-Denti, "Stomatal ozone fluxes over a barley field in Italy. "Effective exposure" as a possible link between exposure- and flux-based approaches," *Atmospheric Environment*, vol. 38, no. 15, pp. 2421–2432, 2004.

[43] H. Akimoto, "Global air quality and pollution," *Science*, vol. 302, no. 5651, pp. 1716–1719, 2003.

[44] J. N. Cape, "Surface ozone concentrations and ecosystem health: past trends and a guide to future projections," *Science of the Total Environment*, vol. 400, no. 1–3, pp. 257–269, 2008.

[45] C. Dueñas, M. C. Fernández, S. Cañete, J. Carretero, and E. Liger, "Assessment of ozone variations and meteorological effects in an urban area in the Mediterranean Coast," *Science of The Total Environment*, vol. 299, no. 1–3, pp. 97–113, 2002.

[46] S. Fares, R. Weber, J.-H. Park, D. Gentner, J. Karlik, and A. H. Goldstein, "Ozone deposition to an orange orchard: partitioning between stomatal and non-stomatal sinks," *Environmental Pollution*, vol. 169, pp. 258–266, 2012.

[47] A. A. Turnipseed, S. P. Burns, D. J. P. Moore, J. Hu, A. B. Guenther, and R. K. Monson, "Controls over ozone deposition to a high elevation subalpine forest," *Agricultural and Forest Meteorology*, vol. 149, no. 9, pp. 1447–1459, 2009.

[48] M. Wesely and B. B. Hicks, "A review of the current status of knowledge on dry deposition," *Atmospheric Environment*, vol. 34, no. 12–14, pp. 2261–2282, 2000.

[49] A. Alimissis, K. Philippopoulos, C. G. Tzanis, and D. Deligiorgi, "Spatial estimation of urban air pollution with the use of artificial neural network models," *Atmospheric Environment*, vol. 191, pp. 205–213, 2018.

[50] C. G. Tzanis, A. Alimissis, K. Philippopoulos, and D. Deligiorgi, "Applying linear and nonlinear models for the estimation of particulate matter variability," *Environmental Pollution*, vol. 246, pp. 89–98, 2019.

[51] D. Fowler, K. Pilegaard, M. A. Sutton et al., "Atmospheric composition change: ecosystems-Atmosphere interactions,"

Atmospheric Environment, vol. 43, no. 33, pp. 5193–5267, 2009.

[52] S. Fares, A. Conte, and A. Chabbi, "Ozone flux in plant ecosystems: new opportunities for long-term monitoring networks to deliver ozone-risk assessments," *Environmental Science and Pollution Research*, vol. 25, no. 9, pp. 8240–8248, 2018.

[53] G. Gerosa, F. Derghi, and S. Cieslik, "Comparison of different algorithms for stomatal ozone flux determination from micrometeorological measurements," *Water, Air, and Soil Pollution*, vol. 179, no. 1–4, pp. 309–321, 2007.